Domain-specific mechanical modulation of VWF–ADAMTS13 interaction

Zhenhai Li[a,b,†], Jiangguo Lin[a,c,†], Todd Sulchek[a,d], Miguel A. Cruz[e], Jianhua Wu[c], Jing-fei Dong[f], and Cheng Zhu[a,d,*]

[a]Coulter Department of Biomedical Engineering and [d]Woodruff School of Mechanical Engineering, Georgia Institute of Technology, Atlanta, GA 30332; [b]Shanghai Institute of Applied Mathematics and Mechanics, Shanghai Key Laboratory of Mechanics in Energy Engineering, Shanghai University, Shanghai 200072, People's Republic of China; [c]Institute of Biomechanics and School of Biology and Biological Engineering, South China University of Technology, Guangzhou, Guangdong 510006, China; [e]Cardiovascular Research Section, Department of Medicine, Baylor College of Medicine, Houston, TX 77030; [f]BloodWorks Northwest Research Institute, Seattle, WA 98102

ABSTRACT **Hemodynamic forces activate the Von Willebrand factor (VWF) and facilitate its cleavage by a disintegrin and metalloprotease with thrombospondin motifs-13 (ADAMTS13), reducing the adhesive activity of VWF. Biochemical assays have mapped the binding sites on both molecules. However, these assays require incubation of two molecules for a period beyond the time allowed in flowing blood. We used a single-molecule technique to examine these rapid, transient, and mechanically modulated molecular interactions in short times under forces to mimic what happens in circulation. Wild-type ADAMTS13 and two truncation variants that either lacked the C-terminal thrombospondin motif-7 to the CUB domain (MP-TSP6) or contained only the two CUB domains (CUB) were characterized for interactions with coiled VWF, flow-elongated VWF, and a VWF A1A2A3 tridomain. These interactions exhibited distinctive patterns of calcium dependency, binding affinity, and force-regulated lifetime. The results suggest that 1) ADAMTS13 binds coiled VWF primarily through CUB in a calcium-dependent manner via a site(s) outside A1A2A3, 2) ADAMTS13 binds flow-extended VWF predominantly through MP-TSP6 via a site(s) different from the one(s) at A1A2A3; and 3) ADAMTS13 binds A1A2A3 through MP-TSP6 in a Ca^{2+}-dependent manner to autoinhibit another Ca^{2+}-independent binding site on CUB. These data reveal that multiple sites on both molecules are involved in mechanically modulated VWF–ADAMTS13 interaction.**

Monitoring Editor
Mark H. Ginsberg
University of California, San Diego

Received: Jan 10, 2019
Revised: Apr 9, 2019
Accepted: May 2, 2019

INTRODUCTION

The multimeric plasma glycoprotein Von Willebrand factor (VWF) mediates platelet adhesion to the subendothelium at sites of vascular injury by interacting with the glycoprotein (GP) Ib-IX-V complex and GPIIb-IIIa on platelets (De Marco *et al.*, 1986; Franchini and Lippi, 2006). The adhesive activity of VWF correlates with the multimer's size, which is in part regulated proteolytically by the zinc metalloprotease a disintegrin and metalloprotease with thrombospondin motifs-13 (ADAMTS13). Deficiency in ADAMTS13 results in accumulation of hyperactive ultralarge (UL) VWF, leading to disseminated platelet-rich microthrombosis in the microvasculature, as seen in patients with thrombotic thrombocytopenic purpura (TTP; Tsai, 2007).

ADAMTS13 consists of an N-terminal metalloprotease domain, a disintegrin-like domain, a TSP1 motif, a cysteine-rich domain, a spacer domain, seven additional TSP1 domains, and two CUB domains at the C-terminus (Zheng *et al.*, 2001; Figure 1A). ADAMTS13 specifically cleaves the Tyr^{1605}-Met^{1606} peptide bond in the VWF A2 domain (Furlan *et al.*, 1996). The cleavage converts the prothrombotic ULVWF to smaller and less adhesive, but hemostatically critical VWF multimers in the circulation (Dong, 2005). The Tyr^{1605}-Met^{1606} peptide bond is buried in the tertiary structure of the A2 domain

This article was published online ahead of print in MBoC in Press (http://www.molbiolcell.org/cgi/doi/10.1091/mbc.E19-01-0021) on May 8, 2019.

†These authors contributed equally to this work.

The authors declare no competing financial interests.

*Address correspondence to: Cheng Zhu (cheng.zhu@bme.gatech.edu).

Abbreviations used: ADAMTS13, a disintegrin and metalloprotease with thrombospondin motifs-13; CUB, ADAMTS13 containing only the two CUB domains; MP-TSP6, ADAMTS13 lacking the C-terminal thrombospondin motif-7 to the CUB domain; VWF, Von Willebrand factor.

© 2019 Li, Lin, *et al.* This article is distributed by The American Society for Cell Biology under license from the author(s). Two months after publication it is available to the public under an Attribution–Noncommercial–Share Alike 3.0 Unported Creative Commons License (http://creativecommons.org/licenses/by-nc-sa/3.0).

"ASCB®," "The American Society for Cell Biology®," and "Molecular Biology of the Cell®" are registered trademarks of The American Society for Cell Biology.

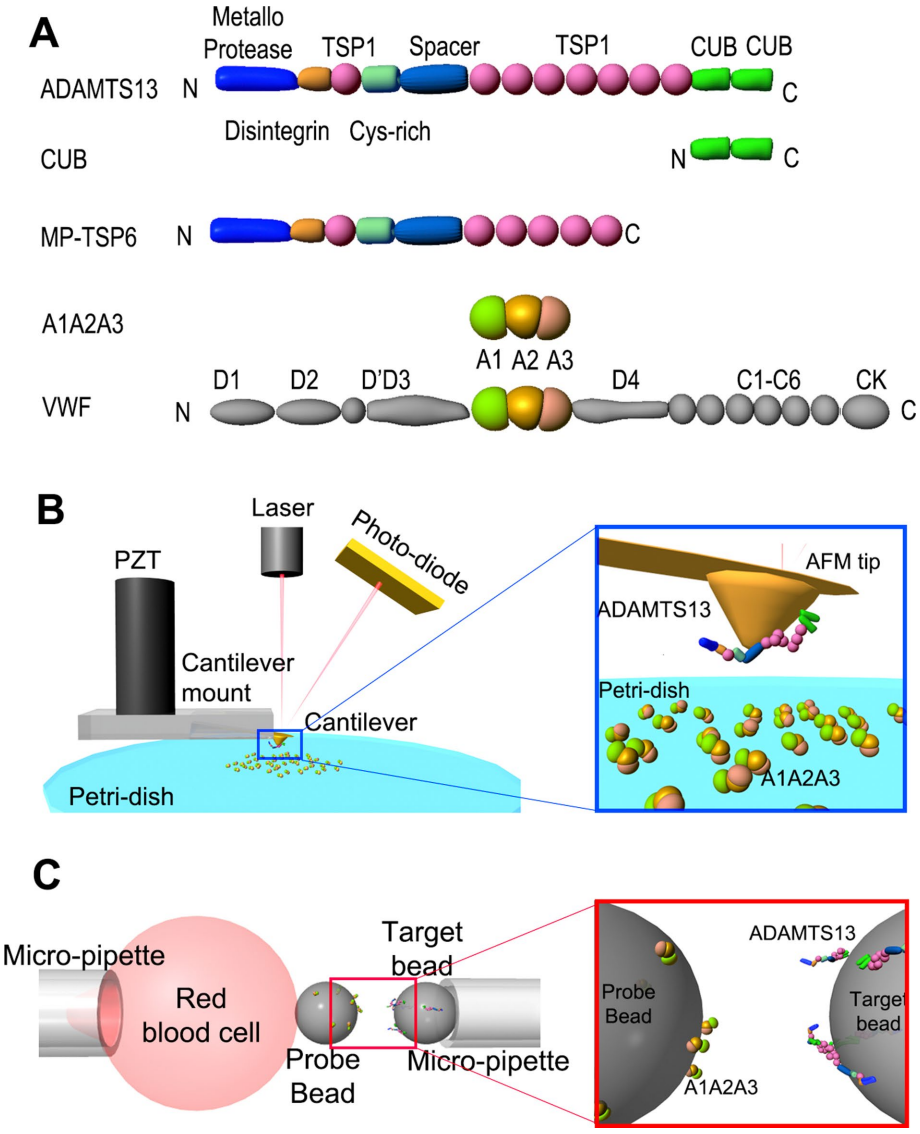

FIGURE 1: Experimental setup. (A) Domain diagrams of the ADAMTS13 variants, A1A2A3, and VWF monomer. (B) AFM schematic and functionalization (not to scale). A cantilever was mounted on a PZT above the polystyrene surface. Its deflection was measured by a laser beam reflected by the back of the cantilever tip onto a photodiode. ADAMTS13 and VWF variants were respectively adsorbed on the cantilever tip and polystyrene surface. (C) BFP schematic and functionalization (not to scale). Two micropipettes respectively aspirate an RBC on the left and a target bead on the right. The probe bead is attached to the apex of the RBC. The deformation of the RBC is measured by tracking the image of the probe bead. A1A2A3 was covalently linked to the probe beads, and the ADAMTS13 variants were adsorbed onto target beads.

(Zhang *et al.*, 2009) as well as in the quaternary structures of the A1A2A3 tridomain polypeptide (Wu *et al.*, 2010) and the VWF multimer (Dong, 2005). This cryptic site can be exposed by hemodynamic forces to facilitate or enhance VWF proteolysis by ADAMTS13 (Furlan *et al.*, 1996; Tsai, 1996). On one hand, a recombinant truncated ADAMTS13 lacking the C-terminal TSP1 and CUB domains remains active in cleaving VWF under static conditions (Zheng *et al.*, 2003; Feys *et al.*, 2009), indicating that these C-terminal domains are not required for ADAMTS13 activity. On the other hand, cooperation between the middle C-terminal TSP1 repeats and the distal C-terminal CUB domains is required for ADAMTS13 to recognize VWF under flow conditions (Zhang *et al.*, 2007) and to downregulate thrombus formation in vivo (Banno *et al.*, 2009).

The apparent discrepancies suggest that ADAMTS13 may interact with VWF multimers in ways undetectable by conventional and biochemical means under static conditions with a long incubation. Prolonged incubation is unlikely to be physiologically permissible, because circulating VWF and ADAMTS13 interact rapidly and transiently in flowing blood. Here we utilized adhesion frequency and force-clamp experiments with atomic force probe (AFM) and biomembrane force probe (BFP) (Figure 1, B and C) to measure force-free or force-modulated binding kinetic rates at distinctive binding sites between ADAMTS13 or its truncation variants and VWF or A1A2A3 with short contacts.

RESULTS

To study the rapid, transient, and mechanically modulated binding of ADAMTS13 to VWF, we made recombinant full-length human ADAMTS13 and two truncation variants, MP-TSP6 (from the N-terminal to the sixth TSP motif), which preserves nearly the same cleavage activity as full-length ADAMTS13 in vitro (Banno *et al.*, 2004), and CUB (two C-terminal CUB domains), which inhibits ADAMTS13 cleavage activity (Tao *et al.*, 2005; Muia *et al.*, 2014; South *et al.*, 2014; Figure 1A). The activity of the recombinant ADAMTS13 and the functionality of plasma VWF and A1A2A3 were confirmed by ADAMTS13 proteolytic assays (Supplemental Figure S1).

ADAMTS13 binds coiled VWF via CUB in a divalent cation-dependent manner

We used AFM to measure the adhesion frequency between ADAMTS13 constructs and VWF at contact time 2 s to mimic the interaction under blood flow, but sufficiently long to reach steady-state binding (see Figure 4B later in the paper). No cleavage product was detected by incubating recombinant ADAMTS13 and VWF multimers for 30 min in the presence of 1 mM of urea (Supplemental Figure S1B), suggesting that cleavage is unlikely to occur during the short contact of 2 s. The nonspecific adhesion between ADAMTS13 (or its truncation variants) and BSA was <4% (Figure 2A, gray boxes), indicating that adhesions with much higher frequencies (>20%) were predominately mediated by specific VWF–ADAMTS13 interaction. Under static conditions, most VWF assumed a coiled conformation (Figure 2, C and D, first column, and F, brown box). Therefore, binding was considered to occur between the coiled VWF and ADAMTS13.

Because the adhesion frequency depends on the binding affinity, the contact area, and the molecular densities of the enzyme and the substrate (see *Materials and Methods*), in the experiments testing the VWF–ADAMTS13, VWF–MP-TSP6, and VWF–CUB binding, we kept the same coating concentrations of ADAMTS13 constructs and

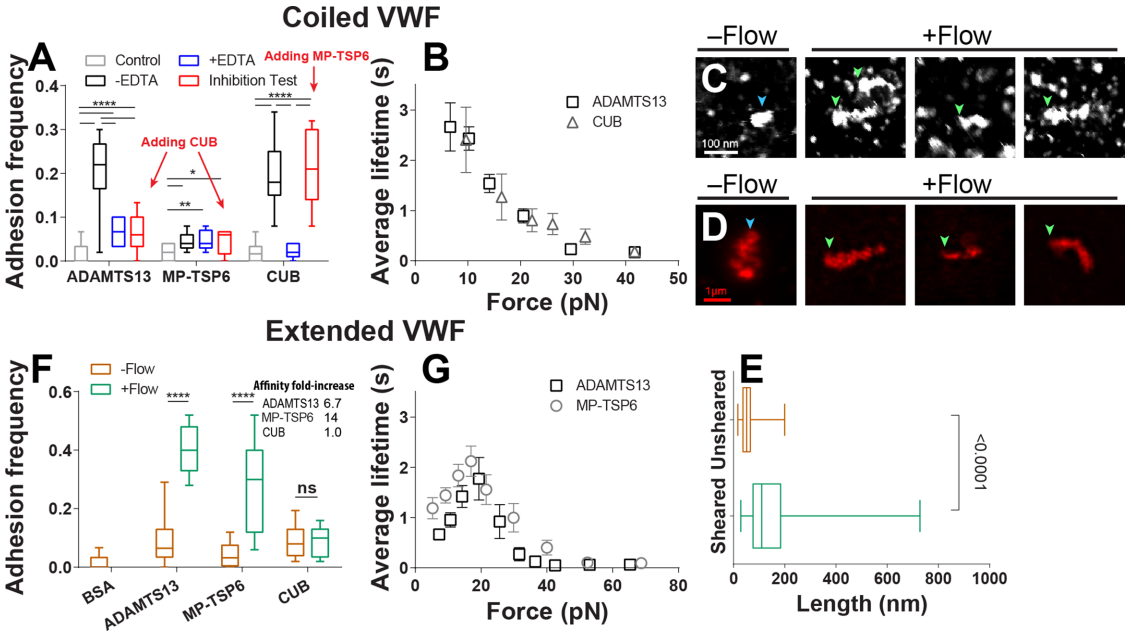

FIGURE 2: Binding characteristics of coiled and flow-extended VWF to ADAMTS13 variants. (A) Adhesion frequencies (median ± quarter percentile and max/min of 5–29 tip-surface spot pairs of 50 contacts each) resulted from 2 s contact of AFM tips bearing ADAMTS13 variants with BSA (gray boxes) or VWF-coated polystyrene surface in the absence (black boxes) or presence (blue boxes) of 5 mM EDTA or in the presence of 10 μg/ml soluble ADAMTS13 variants as indicated (red boxes). $n = 27, 26, 12, 29, 11, 5, 5, 5, 8, 18, 5, 13$ spots were tested for the adhesion frequencies. The statistical analysis results are reported only if the differences are significant. (B) Lifetimes of bonds between plasma VWF and ADAMTS13 (black squares) or CUB (gray triangles) were measured by AFM force-clamp assay and plotted vs. force. Data are presented as mean ± SEM of several tens to several hundreds of measurements per point. (C) AFM scanning images of plasma VWF before (first column) or after (second to fourth columns) experiencing 8000 s^{-1} wall shear rate for 10 min. (D) Superresolution images of plasma VWF before (first column) or after (second to fourth columns) experiencing high shear. Blue and green arrows indicate the coiled and extended VWF in C and D, respectively. (E) Quantitation of VWF lengths along the long axes from AFM images (median ± quarter percentile and max/min of >90 measurements each). (F) Adhesion frequencies (median ± quarter percentile and max/min of $n = 27, 5, 20, 10, 28, 15, 21, 10$ pairs of spots at 50 contacts each) resulted from 0.8 s contact of AFM tips bearing ADAMTS13 variants with BSA (first box), low concentration (2.5 μg/ml) VWF-coated polystyrene surface before flow (brown boxes) or after flow (green boxes). The estimated affinity fold increase is labeled in the figure. (G) Lifetimes of elongated plasma VWF bonds with ADAMTS13 (black squares) or MP-TSP6 (gray circles) were measured by AFM force-clamp assay and plotted vs. force. Data are presented as mean ± SEM of several tens to several hundreds of measurements per point.

VWF (see *Materials and Methods*). Assuming that the contact area was the same, we could compare the affinities of three ADAMTS13 constructs to the coiled VWF. In the presence of Ca^{2+}, coiled VWF bound comparably to ADAMTS13 and CUB (Figure 2A, black boxes). In contrast, VWF–MP-TSP6 binding was higher than for the negative control. Adding EDTA eliminated VWF–CUB binding, but did not affect VWF–MP-TSP6 binding, and reduced VWF–ADAMTS13 binding to the level of VWF–MP-TSP6 binding (Figure 2A, blue boxes). Adding CUB to the reaction solution reduced VWF–ADAMTS13 binding to the level of VWF–MP-TSP6 binding but did not affect VWF–MP-TSP6 binding, whereas adding MP-TSP6 had no effect on VWF–CUB binding (Figure 2A, red boxes). These data suggest that ADAMTS13 binding to VWF multimers under static conditions was primarily through the CUB domains and required divalent cations.

We next measured lifetimes of VWF–ADAMTS13 and VWF–CUB bonds under force with AFM to further define their characteristics. Both VWF–ADAMTS13 and VWF–CUB bonds displayed indistinguishable slip-bond characteristics, where the bond lifetime decreased with increasing force (Marshall *et al.*, 2003; Yago *et al.*, 2004; Figure 2B). These force-dependent bond lifetimes corroborate the adhesion frequency data, suggesting that ADAMTS13 binds to coiled VWF multimers through the CUB domains under static conditions.

ADAMTS13 binds flow-extended VWF via MP-TSP6 with a much higher affinity than and a distinct force-dependent bond lifetime pattern from that via CUB

It has been shown that shear flow can elongate globular VWF multimers (Schneider *et al.*, 2007). To investigate ADAMTS13 binding to shear-extended VWF, we immobilized a low density of VWF on the Petri dish surface precoated with a high density of a polyclonal antibody, then exposed the surface to a high fluid shear stress to elongate VWF. VWF was unable to recoil back after the flow was stopped, as it was further captured on additional points by the excessive antibody (Supplemental Figure S3). Fluorescence-conjugated VWF appeared as isolated round spots imaged by both AFM (Figure 2C, first column) and superresolution microscopy (SIM) (Gustafsson, 2005; Figure 2D, first column) without shear, but became elongated stringlike structures after long shear exposure (8000 s^{-1} for 10 min; Figure 2, C and D, second to fourth columns). The length of VWF along the long axes in AFM images increased threefold ($p < 0.0001$) after exposure to shear stress (Figure 2E).

Regardless of the difference of protein densities, the two sets of data (Figure 2, A, black boxes, and F, brown boxes) showed the same qualitative pattern: comparable levels of VWF binding to ADAMTS13 and CUB, which were higher than that to MP-TSP6.

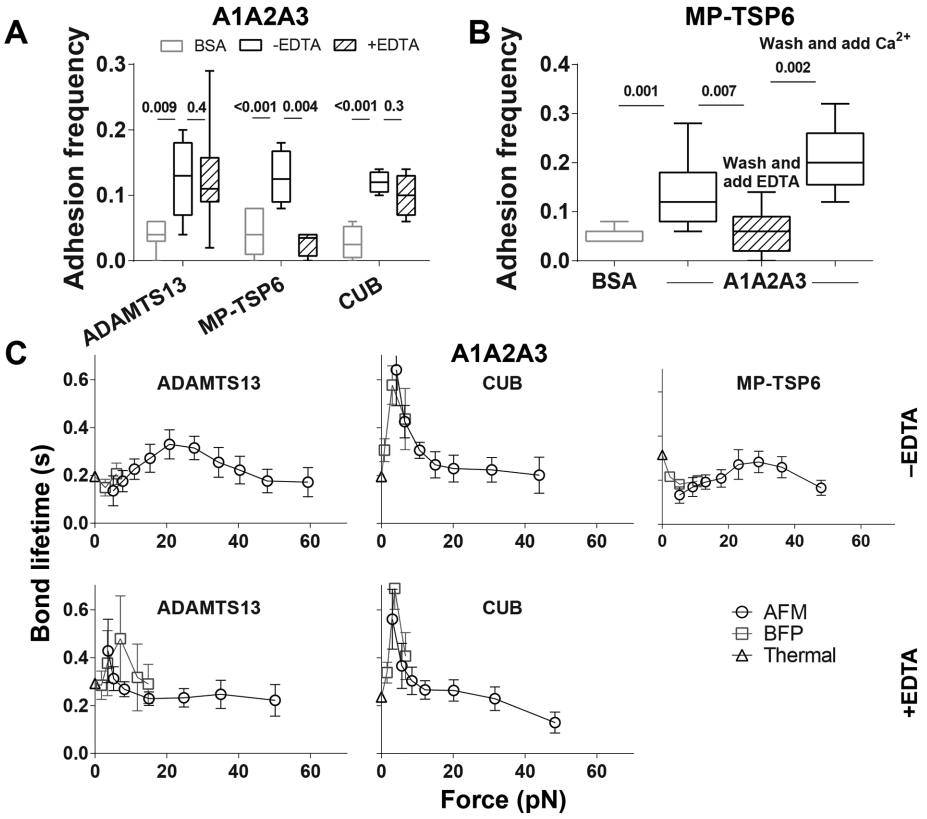

FIGURE 3: Binding characteristics of A1A2A3 to ADAMTS13 variants. (A) Adhesion frequencies (median ± quarter percentile and max/min of $n = 6, 9, 12, 5, 4, 4, 4, 4, 4$ tip-surface spot pairs of 50 contacts each) resulted from 0.8 s contact of AFM tips bearing ADAMTS13 variants with BSA (open gray boxes) or A1A2A3-coated polystyrene surface in the absence (open black boxes) or presence (hatched boxes) of 5 mM EDTA. (B) Adhesion frequencies (median ± quarter percentile and max/min of $n = 9, 11, 9, 10$ tip-surface spot pairs of 50 contacts each) resulted from 0.8 s contact using MP-TSP6-bearing AFM tip sequentially to 1) BSA (first box), 2) A1A2A3-coated polystyrene surface (second box), 3) A1A2A3 surface with EDTA in the solution (third box), and 4) A1A2A3 surface after EDTA was washed out and 5 mM Ca^{2+} was added to the solution (fourth box). The *p* values obtained from Student's *t* test are labeled on top of the bars. (C) Lifetimes of A1A2A3 bonds with indicated ADAMTS13 variants were measured by AFM (open circles) or BFP (open squares) force-clamp assay or BFP thermal fluctuation assay (open triangles) in the absence (top row) or presence (bottom row) of 5 mM EDTA and plotted vs. force. Data are presented as mean ± SEM of several tens to several hundreds of measurements per point.

These data also suggest that differences in conformation between directly adsorbed and antibody-captured VWF molecules on the surface, if any, do not detectably impact their binding to ADAMTS13 and its truncation variants. Remarkably, shear-elongated VWF showed greatly enhanced binding to ADAMTS13 and MP-TSP6, but not to CUB (Figure 2F, green boxes). Using the same coating concentration of the ADAMTS13 constructs and VWF, we expected the same molecular densities of the enzyme and substrate, respectively. The changes in affinity were calculated from the increases in adhesion frequencies (see *Materials and Methods*). ADAMTS13 and MP-TSP6 showed respectively 6.7- and 14-fold higher affinities for the flow-extended than for the coiled VWF captured by antibodies. These results suggest that, instead of binding to the CUB domains, elongated VWF exposes a new site for ADAMTS13, and this new site binds to MP-TSP6 with a much higher affinity than the coiled VWF–CUB binding affinity (Figure 2F).

We also compared the force-dependent lifetimes of elongated VWF–MP-TSP6 and elongated VWF–ADAMTS13 bonds by AFM. Both interactions exhibited indistinguishable catch-slip bonds, where the bond lifetime first increased with force until reaching a peak, and then decreased as force further increased (Marshall *et al.*, 2003; Yago *et al.*, 2004; Figure 2G), showing a pattern qualitatively distinct from that of the slip bond of the coiled VWF interactions with ADAMTS13 and with CUB (Figure 2B). The bond lifetime measurements corroborated with the adhesion frequency measurements, strongly indicating that elongated VWF interacts primarily with ADAMTS13 through a site on MP-TSP6. The zero-force extrapolation of the extended VWF–ADAMTS13 bond lifetime is much shorter than that of the coiled VWF–ADAMTS13 bond lifetime (Figure 2, B and G), indicating a much faster off-rate for ADAMTS13 dissociation from flow-extended than from coiled VWF. Combined with affinity differences, the finding translates to an order of magnitude–faster on-rate for ADAMTS13 to associate with flow-extended than coiled VWF.

A1A2A3 and VWF bind ADAMTS13 through different sites

To further dissect the binding site for MP-TSP6, which is exposed only on elongated VWF multimers, we analyzed the binding of a VWF A1A2A3 polypeptide to the ADAMTS13 constructs. A1A2A3 contains the sites for VWF interactions with glycoprotein Ibα (GPIbα) on platelets (A1) and collagen in the subendothelial matrix (A1 and A3), as well as the peptide bond cleaved by ADAMTS13 (A2) (Ruggeri and Mendolicchio, 2015). A1A2A3 is thought to be buried in coiled VWF, but becomes exposed upon VWF extension by shear stress. The adhesion frequency between an ADAMTS13 and an A1A2A3 was specific and not affected by EDTA (Figure 3A). A1A2A3–MP-TSP6 binding is similar to that of A1A2A3–ADAMTS13 in the presence of Ca^{2+}, but was abolished by EDTA (Figure 3A). The Ca^{2+}-dependence of the A1A2A3–MP-TSP6 binding was confirmed when the reaction buffer was recalcified (Figure 3B). The different divalent cation requirements for A1A2A3 to bind MP-TSP6 and full-length ADAMTS13 suggest the presence of another A1A2A3 binding site outside MP-TSP6. This prediction was confirmed by the specific and divalent cation-independent binding between CUB and A1A2A3 (Figure 3A). Thus, ADAMTS13 contains two binding sites for A1A2A3: one on MP-TSP6 that is calcium-dependent and the other on the CUB domains that is calcium-independent. The divalent-cation dependencies of A1A2A3 interactions with the three ADAMTS13 constructs (Figure 3A) are opposite to those of the coiled VWF (Figure 2A), suggesting that A1A2A3 and coiled VWF bind ADAMTS13 using distinct binding sites.

The two ADAMTS13 binding sites for A1A2A3 exhibit distinct force-dependent bond lifetimes

The calcium requirement for A1A2A3 binding to MP-TSP6, but not to ADAMTS13 and CUB (Figure 3A), implies that ADAMTS13 used

CUB to bind A1A2A3 when Ca^{2+} was chelated. When Ca^{2+} was present, however, it was not clear whether A1A2A3 bound to MP-TSP6, CUB, or both. To address this question, we compared the force-dependent lifetimes of bonds between A1A2A3 and ADAMTS13 in the presence and absence of EDTA. In the presence of Ca^{2+}, lifetimes of A1A2A3–ADAMTS13 (Figure 3C, top left) and A1A2A3–MP-TSP6 (Figure 3C, top right) bonds showed similar triphasic force dependency: first decreasing, followed by a modest increase, and then decreasing. This pattern of slip–catch–slip bonds has previously been reported for E-selectin–ligand (Wayman *et al.*, 2010) and VWF A1–GPIbα (Ju *et al.*, 2013) interactions. In contrast, the A1A2A3–CUB interaction behaved as catch–slip bonds (Marshall *et al.*, 2003; Yago *et al.*, 2004) (Figure 3C, top middle). These data indicate that in the presence of Ca^{2+}, ADAMTS13 binds A1A2A3 through a binding site on MP-TSP6, as the binding site on CUB makes no detectable contribution to the measured A1A2A3–ADAMTS13 binding properties.

We next compared the lifetime versus force curves of the A1A2A3 bonds with ADAMTS13 and CUB under distinct cation conditions. The A1A2A3–CUB bond lifetime versus force curve was not changed by chelating calcium (Figure 3C, top and bottom middle). By comparison, the triphasic lifetime versus force curve of the A1A2A3–ADAMTS13 bond (Figure 3C, top left) was converted to a biphasic curve when divalent cations were chelated by EDTA (Figure 3C, bottom left), which was comparable to the A1A2A3–CUB bond lifetime curve (Figure 3C, bottom middle). These data further confirmed that ADAMTS13 binds through a binding site on CUB to A1A2A3 in the absence of divalent cations. The force-dependent lifetime curves of A1A2A3 bonds with the three ADAMTS13 constructs (Figure 3C) are distinct from those of the coiled and flow-extended VWF (Figure 2, B and G), again, ruling out the possibility that A1A2A3 uses sites identical to either form of VWF to bind ADAMTS13, MP-TSP6, or CUB.

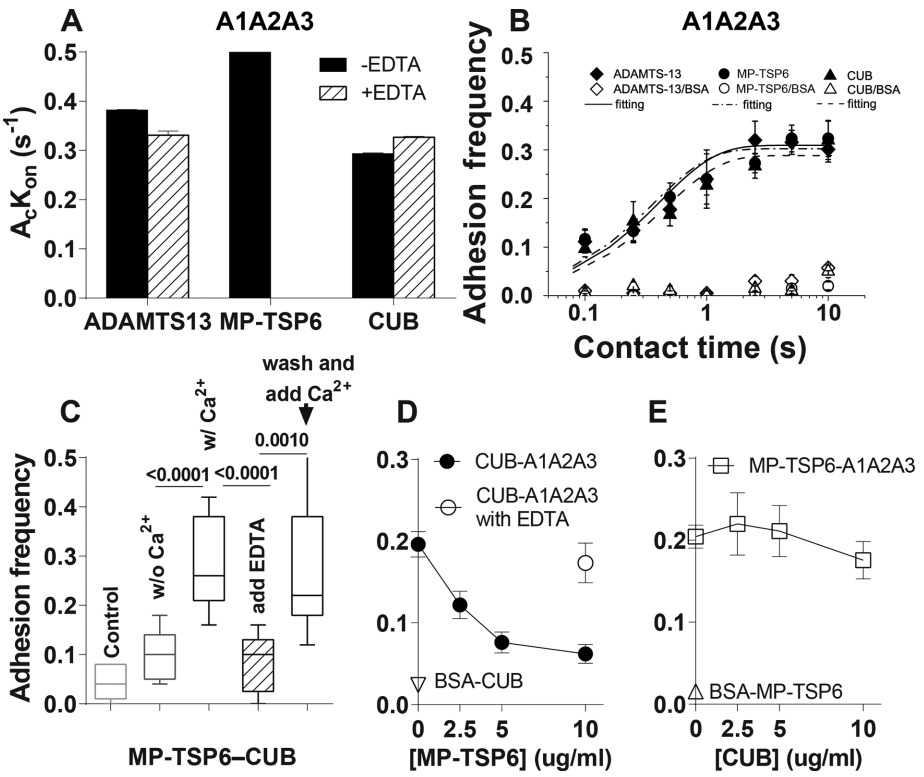

FIGURE 4: Binding kinetics and inhibition. (A) 2D effective on rates (mean ± SEM of 3–6 bead pairs making 30 contacts of 900–1800 s total contact time, several tens to several hundreds of waiting time events) of A1A2A3 association with indicated ADAMTS13 variants measured by BFP thermal fluctuation assay. (B) Adhesion frequencies of 50 contacts (mean ± SEM of $n = 6$–12 tip–surface spot pairs per positive data point and $n = 4$ per negative control data point) of AFM tips (bearing indicated ADAMTS13 variants) with BSA (open symbols)- or A1A2A3 (closed symbols)-coated polystyrene surfaces were plotted against contact time and fitted by Eq. 1 (curves). (C) Adhesion frequencies (median ± quarter percentile and max/min of $n = 5$, 9, 10, 8, 11 tip–surface spot pairs of 50 contacts each) at 5 s contact time of MP-TSP6-bearing AFM tips to 1) BSA surface (first box), 2) CUB surface (second box), 3) CUB surface with EDTA in the solution (third box), and 4) CUB surface after EDTA was washed out and 5 mM Ca^{2+} was added (fourth box). (D) Solution MP-TSP6 inhibited CUB binding to A1A2A3 in a cation- and dose-dependent manner (circles.). Nonspecific binding of AFM tips coated with MP-TSP6 (triangles) to BSA-coated surfaces serves as negative control. (E) Solution CUB did not inhibit MP-TSP6 binding to A1A2A3 (squares). Nonspecific binding of AFM tips coated with CUB (inverted triangles) to BSA-coated surfaces serves as negative control. Data in D and E are presented as mean ± SEM of 6–15 tip–surface spot pairs of 50 5-s contacts each.

MP-TSP6 binding inhibits CUB–A1A2A3 binding, but not vice versa

The results presented so far have led to two hypotheses: 1) MP-TSP6 has a much higher on-rate than CUB for A1A2A3 and 2) A1A2A3–CUB binding is autoinhibited in native ADAMTS13. To test the first hypothesis, we directly compared the on-rate of A1A2A3 association with ADAMTS13 or its truncation variants in the presence and absence of EDTA using a thermal fluctuation assay with BFP (Chen *et al.*, 2008a,b) and an adhesion frequency assay (Chesla *et al.*, 1998; Chen *et al.*, 2008b) with AFM. The thermal fluctuation assay measured the apparent effective 2D on-rates A_ck_{on} and zero-force off-rates k_{off}^0 of A1A2A3 interactions with ADAMTS13, MP-TSP6, and CUB, where A_c is a contact area in the experiment. A_ck_{on} is shown in Figure 4A and listed in Table 1. A1A2A3 had comparable effective 2D on-rates for ADAMTS13 and MP-TSP6 in the presence of calcium, while its on-rate for CUB was independent of divalent cations. The frequency versus contact time curves of A1A2A3 adhesion to ADAMTS13, MP-TSP6, and CUB are also indistinguishable (Figure 4B). These results rejected the first hypothesis.

To test the second hypothesis, we first measured the adhesion frequency of MP-TSP6 to CUB in the presence of Ca^{2+} at contact time 5 s. The adhesion was minimal until Ca^{2+} was added to the buffer. The binding was abolished by EDTA and rescued by recalcification (Figure 4C), suggesting the possibility of inhibition of one binding site by the other for A1A2A3 binding.

We next tested whether the binding of A1A2A3 by one ADAMTS13 truncation variant could be inhibited by the other ADAMTS13 truncation variant in solution. Interestingly, soluble MP-TSP6 inhibited the A1A2A3–CUB interaction in a dose-dependent manner (Figure 4D, black circle line),

	AFM		BFP	
	$m_r m_l A_c K_a$	k^0_{off} (s^{-1})	$A_c K_a$	k^0_{off} (s^{-1})
ADAMTS13	0.31 ± 0.02	2.28 ± 0.48	0.382 ± 0.001	4.28 ± 0.11
MP-TSP6	0.34 ± 0.02	2.39 ± 0.52	0.520 ± 0.008	4.20 ± 0.04
CUB	0.32 ± 0.02	1.91 ± 0.44	0.296 ± 0.002	6.09 ± 0.14

Kinetic parameters from AFM adhesion frequency assay were derived from fitting Eq. 1 to the adhesion frequency vs. contact time data. Kinetic parameters from BFP thermal fluctuation assay were derived from fitting Eq. 2 to the waiting time and bond lifetime distributions.

TABLE 1. Kinetic parameters of ADAMTS13 constructs binding to A1A2A3.

whereas the A1A2A3–MP-TSP6 interaction was not affected by the addition of CUB (Figure 4E, open square line). Moreover, the inhibitory effect of soluble MP-TSP6 on A1A2A3–CUB interaction was abolished by 5 mM of EDTA (Figure 4D, open circle), further supporting the assertion that the inhibition of CUB by MP-TSP6 requires calcium-dependent binding of soluble MP-TSP6 to CUB on the cantilever, A1A2A3 on the surface, or both. Together, these data have provided strong support for autoinhibition between the two ADAMTS13 binding sites for A1A2A3.

DISCUSSION

Hemodynamic forces in the circulation stretch ULVWF or immobilized VWF to a more extended configuration to enhance platelet binding, which may induce thrombosis formation (Schneppenheim *et al.*, 2019), and to expose the cryptic proteolytic site in the A2 domain for cleavage by ADAMTS13 (Furlan *et al.*, 1996; Tsai, 1996; Zhang *et al.*, 2009; Wu *et al.*, 2010), which may reduce VWF activity. Here we further demonstrated that mechanical forces modulate VWF–ADAMTS13 interaction when the enzyme and the substrate come into rapid, repetitive, but brief contacts, which is likely to occur in flowing blood.

The mechanical modulation studied here includes two aspects. One is mechanical modulation of the dissociation kinetics of ADAMTS13 or its truncation variants from either coiled or flow-extended VWF, as well as the A1A2A3 tridomain, under different divalent conditions. In particular, we found that these interactions exhibit multiple bond characteristics: slip bonds, catch bonds, biphasic bonds, and triphasic bonds that depend on the divalent cation conditions and are site-specific, which has not been previously demonstrated in enzyme–substrate interaction. These dynamic bonds may be critical for the regulation of the ADAMTS13 interaction with, and subsequent cleavage of, VWF, as such interaction can be mechanically strengthened or weakened by the formation of various dynamic bonds between the different binding sites in the circulation where comparable mechanical forces are present.

The second aspect of mechanical modulation is shifting of the ADAMTS13 binding site(s) from CUB to MP-TSP6 by shear-induced extension of VWF. Here we used biophysical characteristics as mechanical signatures to distinguish different binding sites between ADAMTS13 or its truncation variants and coiled or flow-extended VWF or A1A2A3. We found that ADAMTS13 binds to coiled VWF primarily through CUB. This finding is consistent with the previous report that the C-terminus of ADAMTS13 binds to a constitutively exposed binding site on the D4 domain of the globular VWF surface (Zanardelli *et al.*, 2009). We also found that, when VWF is anchored, it could be extended by shear flow to allow rapid ADAMTS13 binding through MP-TSP6 with greatly increased affinity. This finding is consistent with the previous report that discontinuous exosites in the disintegrin to spacer domains only bind extended VWF (Gao *et al.*, 2006, 2008; Akiyama *et al.*, 2009; de Groot *et al.*, 2009). The significance of this second aspect of mechanical modulation of VWF–ADAMTS13 interaction is illustrated by drastically increased kinetic on and off rates of the binding under flow conditions.

The A1A2A3–CUB interaction is inhibited in intact ADAMTS13 through an MP-TSP6–CUB interdomain interaction, which may have masked the binding site on CUB for A1A2A3. This finding is consistent with a previously reported conformation of inactive ADAMTS13 (Muia *et al.*, 2014; South *et al.*, 2014) and further suggests that MP-TSP6 may be in an active conformation. In our study, this MP-TSP6–CUB interaction has no detectable effect on the A1A2A3 binding site on MP-TSP6, which is consistent with the previous report that the efficiency of cleavage of the D1596-T1668 region of mouse VWF by mouse ADAMTS13 is comparable to that by mouse ADAMTS13 lacking the two C-terminal TSP1 and two CUB domains (Banno *et al.*, 2004). It is conceivable that the MP-TSP6–CUB interdomain interaction may also exhibit dynamic bond characteristics, allowing hemodynamic forces to modulate the conformational change of ADAMTS13 and facilitate the cleavage of VWF. CUB has been reported to bind the spacer domain, which masks the previously found binding exosites on the spacer domain (Gao *et al.*, 2006; Akiyama *et al.*, 2009; Muia *et al.*, 2019; Zhu *et al.*, 2019). Thus, the A1A2A3 interactions with ADAMTS13 and MP-TSP6 observed in this study may not involve the exosites on the spacer domain. Considering that A1A2A3–MP-TSP6 interaction is Ca^{2+}-dependent and a Ca^{2+}-binding site had been identified in the metalloprotease domain, which is critical to VWF interaction with and cleavage by ADAMTS13 (Gardner *et al.*, 2009), the metalloprotease domain might be involved in the A1A2A3–MP-TSP6 interaction observed in this study. Moreover, a Ca^{2+} binding site was found in the VWF-A2 domain as well, which can stabilize the folded A2 conformation and promote the extended A2 to refold (Xu and Springer, 2012). Thus, the Ca^{2+} dependency of A1A2A3–MP-TSP6 binding may indicate that Ca^{2+} is directly involved in the binding, or this dependency may be introduced by a conformational change in the metalloprotease domain or A2 domain along with the Ca^{2+} condition change. In addition, MP-TSP6–CUB and VWF–CUB binding depends on Ca^{2+}. Future studies will clarify the role of Ca^{2+} in A1A2A3–MP-TSP6 binding.

Combined with recent findings of ADAMTS13 conformational changes (Muia *et al.*, 2014; South *et al.*, 2014, 2017), our data suggest a model of multistep activation of interaction between VWF and ADAMTS13, which prepares the two proteins for proteolytic reaction by a series of activation and binding steps through different sites (Figure 5). Given that VWF assumes a globular conformation under static or low-shear conditions (Schneider *et al.*, 2007), we propose that ADAMTS13 in the autoinhibited conformation may initially bind globular VWF through its CUB domains. The slip bond between CUB and globular VWF may dissociate more rapidly under blood flow; however, blood flow may also elongate tethered VWF and expose its cryptic site(s) for additional ADAMTS13 binding

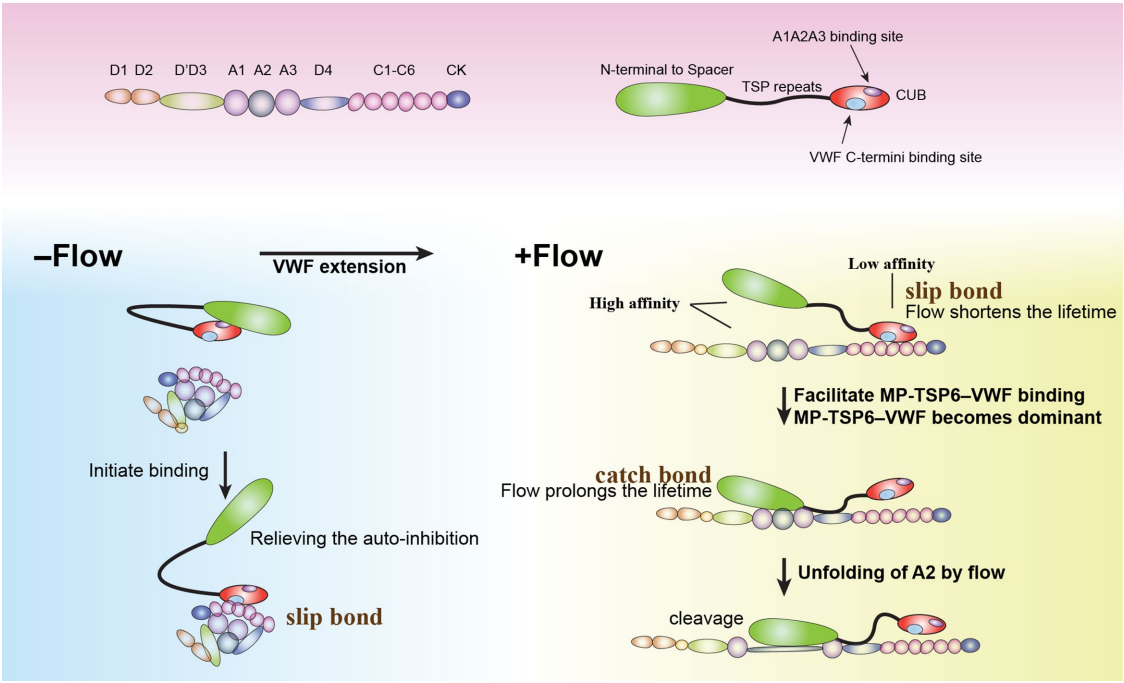

FIGURE 5: ADAMTS13–VWF binding model. ADAMTS13 may bind VWF via different sites depending on their conformations. (Left) Under static or low-flow conditions when VWF is coiled, ADAMTS13 in the autoinhibited conformation may initiate binding through CUB interaction with VWF D4CK. This binding may induce opening of ADAMTS13, relieving the autoinhibitive interaction of CUB with MP-TSP6, enhancing VWF–ADAMTS13 interaction. (Right) In blood flow, tethered VWF may experience high shear stress, forcing it to adopt an elongated conformation and expose cryptic binding sites. ADAMTS13 may shift its binding site for VWF from CUB to MP-TSP6 by binding to the newly exposed binding sites on the extended VWF. This interaction has high affinity and rapid kinetics and can sustain force with catch bonds. Further shear stress exposes more binding sites on A1A2A3 and the cleavage site in the unfolded A2 domain, leading to eventual VWF cleavage.

through MP-TSP6 with a higher affinity and a catch bond characteristic, which may be facilitated by the existing VWF–ADAMTS13 binding through CUB via dimeric interaction (Figure 5). The catch bond between MP-TSP6 and extended VWF may stabilize their interaction under force. The flow-induced extension of VWF may also expose the A1A2A3 tridomain and unfold the A2 domain. The binding of VWF via sites outside A1A2A3 to ADAMTS13 may induce its opening, relieving the autoinhibition of the CUB binding site by MP-TSP6 and allowing ADAMTS13 binding to A1A2A3 via the site on MP-TSP6 and the newly exposed site on CUB. Through such multistep binding involving shifts of sites, ADAMTS13 is well positioned on VWF, assuming an active conformation for the eventual cleavage of the peptide bond in the VWF A2 domain. Our model supports the molecular zipper model (Crawley *et al.*, 2011) and further depicts the binding sites shifting in VWF–ADAMTS13 binding along with the affinity change. Future studies will test this model to further elucidate the detailed process of ADAMTS13 activation, binding and cleavage of VWF under dynamic flow conditions.

MATERIALS AND METHODS

Proteins and antibodies

The recombinant A1A2A3 protein was expressed in mammalian (HEK293) cells and purified from the conditioned medium as previously described (Wu *et al.*, 2010). Its purity and monomeric state were verified by SDS–gel electrophoresis and gel filtration chromatography (Auton *et al.*, 2010). The recombinant cDNAs for wild-type human ADAMTS13, MP-TSP6, and CUB (R75 to T1427, R75 to P1011, and A1191 to T1427) were cloned into the mammalian expression vector pcDNA3.1 with a polyhistidine tag (Cat. # 11040H08B; InVitrogen, Carlsbad, CA) and transfected into CHO cells using lipids as the carrier. ADAMTS13 and its truncation variants were purified from the conditioned medium using Ni-column chromatography as previously described (Tao *et al.*, 2005). The purity of ADAMTS13 is >90% and the activity was confirmed by cleaving plasma VWF and recombinant VWF A1A2A3 (Supplemental Figure S1). Mouse anti-A1 monoclonal antibody (mAb) 5D2 was from Michael Berndt (Curtin University, Australia). Goat anti-ADAMTS13 mAbs 151/158 was from Bethyl Laboratories (Montgomery, TX). Human plasma VWF (Cat. # 681300) was purchased from EMD Biosciences (San Diego, CA). Rabbit anti-VWF polyclonal antibody (Cat. # ab6994) was purchased from Abcam (Cambridge, UK). PE-conjugated goat anti-mouse immunoglobulin G (IgG) (Cat. # sc-3738) and rabbit anti-goat antibody IgG (Cat. # sc-3755) were purchased from Santa Cruz Biotechnology (Dallas, TX). Cyanine5 NHS ester (Cat. # 23020) was purchased from Lumiprobe Corporation (Hunt Valley, MD).

AFM experiments

AFM was used in the adhesion frequency assay for measuring two-dimensional (2D) kinetics at zero force (Chesla *et al.*, 1998; Chen *et al.*, 2008b) and the force-clamp assay for measuring single-bond lifetimes in a range of forces (Marshall *et al.*, 2003; Supplemental Figure S2, A and B).

Our home-built AFM (Figure 1B) and its use for single-molecule experiments have been described previously (Wu *et al.*, 2010). Briefly, AFM cantilevers (MLCT model from Bruker, Billerica, MA)

were functionalized by incubation with various ADAMTS13 variants in buffer (40 µg/ml for each variant, 10 µl per cantilever) at 4°C overnight, rinsed, and soaked in phosphate-buffered saline (PBS) containing 1% bovine serum albumin (BSA) to block nonspecific binding. Polystyrene dishes were cleaned with absolute ethanol and dried with argon gas before protein adsorption. Surfaces were incubated with 15 µl per spot of 1% BSA (for nonspecific control), 40 µg/ml A1A2A3, or 250 µg/ml plasma VWF at 4°C overnight and rinsed three times with PBS. Dishes were then filled with PBS containing 1% BSA in the presence or absence of 5 mM EDTA. For inhibition assays, ADAMTS13 variant-containing buffer (2.5–10 µg/ml) was added to the dish and incubated for 30 min at room temperature before experiments were run. Similarly, for Ca^{2+}-dependency assays, sample was incubated with or without 5 mM Ca^{2+}-containing buffer for 30 min at room temperature before experiments, when conditions changed.

AFM experiments were performed by force ramp for adhesion frequency measurements or force clamp for bond lifetime measurements. A piezoelectric translator (PZT) drove the AFM cantilever to approach and contact the surface (Supplemental Figure S2, A and B, black curves), retracted ~15 nm above the surface to reduce the nonspecific binding (Supplemental Figure S2, A and B, blue curves), held for a given contact time to allow bond formation (Supplemental Figure S2, A and B, green curves), retracted at a speed of 50 pN/s to detect adhesion (Supplemental Figure S2, A and B, red curves), and then this cycle was repeated 50 times to enumerate adhesion frequency for each contact time. For bond lifetime measurements, when adhesion was detected and reached the desired force (Supplemental Figure S2B), the feedback control stopped the PZT movement and maintained the force level until bond dissociation, when the force could no longer be kept at a constant level. In lifetime measurement, proteins were coated at low densities to ensure infrequent adhesions (~20%), a condition previously shown to be necessary for binding at a single-bond level (Chesla *et al.*, 1998). Adhesion frequency and lifetime measurements between different molecular pairs were repeated multiple times with different AFM cantilever tips. Our previous study demonstrated that force-induced conformational change is a prerequisite for A1A2A3 to be cleaved by ADAMTS13 (Wu *et al.*, 2010). To exclude the cleavage events, only single-force-drop events were analyzed in the present study so that the measured lifetime data reflected the dissociation kinetics of bonds between ADAMTS13 variants and A1A2A3 but not the enzymatic kinetic properties of A2 cleavage by ADAMTS13. In addition, we previously observed similar GPIbα binding and ADAMTS13 cleavage properties for both adsorbed and antibody captured A1A2A3 on polystyrene surfaces (Wu *et al.*, 2010), suggesting that adsorption was unlikely to alter the A1A2A3 binding properties to ADAMTS13 constructs.

Extension of VWF by shear flow

The Petri dish or glass surfaces were preincubated with 15 µl per spot of 80 µg/ml polyclonal anti-VWF polyclonal antibody (ab6994) at 4°C overnight and rinsed three times with PBS. In the day of the experiment, surfaces were incubated with 15 µl of plasma VWF with indicated concentration at room temperature for 30 min. A GlycoTech parallel plate flow chamber (Cat. # 31-001; GlycoTech Corporation) was assembled using the plasma VWF coated on the Petri dish surface as the chamber floor. A continuous flow of buffer (viscosity ~1 cP) was applied for 10 min at a wall shear rate of 8000 s^{-1}. The VWF-coated surfaces were recovered. The Petri dishes were used for further AFM adhesion frequency or force clamp experiments. The glass surfaces were scanned with AFM (MFP-3D Stand Alone AFM, Asylum Research, Oxford Instruments), or examined by superresolution fluorescence microscopy (Zeiss LSM 780 and Elyra PS.1, Carl Zeiss Microscopy GMbH) to obtain SIM images (Gustafsson, 2005). The VWF multimers used for superresolution microscopy were preconjugated with a fluorescent dye (Cy5) according to the Lumiprobe protocol.

BFP experiments

BFP was used in the thermal fluctuation assay to measure 2D on/off rates of single bonds at zero force (Chen *et al.*, 2008a,b; Supplemental Figure S2C) and force-clamp assay for measuring single-bond lifetimes at low forces (Chen *et al.*, 2010). The coating density of proteins was controlled to ensure infrequent adhesions (~20%).

Our home-built BFP and its use for single-molecule experiments have been previously described (Chen *et al.*, 2008a,b; Ju *et al.*, 2017). Briefly, two micropipettes, placed in a cell chamber mounted on the stage of an inverted microscope, were used to aspirate a biotinylated red blood cell (RBC) and a target bead, respectively (Figure 1C). A probe bead was attached to the apex of the RBC through biotin–streptavidin coupling using a third micropipette to form a force transducer. The position of the probe was tracked by a high-speed camera (1500 frames per second) with a spatial resolution of a few nanometers. A1A2A3 and streptavidin were covalently linked to probe beads using a previously described chemistry (Chen *et al.*, 2008a). ADAMTS13 variants were coated on target beads by overnight incubation of each variant (400 µg/ml) at room temperature, rinsed with HEPES, and soaked in HEPES with 1% BSA to block nonspecific binding. For experimental testing of Ca^{2+} dependency, both target and probe beads were incubated with or without EDTA for 30 min before the experiment.

Bond lifetimes in the low-force regime were measured by BFP, as it has a much softer (small–spring constant) force transducer than AFM. Nonspecific adhesion in the BFP was controlled using A1A2A3-coated bead and BSA-coated bead, which resulted in a 4% adhesion frequency. The bond lifetime experiment procedures were similar to that described for AFM, except that BFP was used. For the thermal fluctuation assay, the target bead was driven by the PZT to contact the probe bead, retract, and hold at a null position (0 pN) for 10 s. The thermal fluctuation of the probe bead was monitored to identify events of bond formation and dissociation, respectively, from its sudden reduction and resumption of the fluctuation amplitude, gauged through the 90-point sliding SD of the probe bead displacement over time (Supplemental Figure S2C). The thermal fluctuation changed because bond formation between molecules on the two beads restricted the movement of the probe bead. The time it took to form a bond (waiting time) and the time the bond lasted (bond lifetime) were measured and pooled for kinetic analysis.

Kinetic analysis and modeling

After the nonspecific binding was removed, the specific adhesion frequency P_a was fitted by nonlinear regression to a probabilistic kinetic model for single-step monovalent receptor–ligand interaction (Chen *et al.*, 2008b):

$$P_a = 1 - \exp\left(-\langle n \rangle\right) \tag{1a}$$

$$\langle n \rangle = m_{AD} m_{VWF} A_c K_a \left[1 - \exp\left(-k_{off}^0 t_c\right)\right] \tag{1b}$$

where m_{AD} and m_{VWF} denote the densities of the ADAMTS13 and VWF variants, respectively, A_c is the contact area, K_a is the 2D binding affinity, and k_{off}^0 is the off rate. The superscript 0 indicates

the off rate evaluated at zero force to distinguish from those obtained from bond lifetime measurements under force.

To calculate fold increase in affinity (K_a ratio) of the same ADAMTS13 variant for the flow-extended VWF over the coiled VWF, we used the steady state version of Eq. 1 (by letting $t_c \to \infty$) and solved for $m_{AD}m_{VWF}A_cK_a = -\ln(1 - P_a)$. The K_a ratio can be obtained by the ratio of $\ln(1 - P_a)$ calculated from the measured P_a in Figure 2F, because the molecular densities and contact area remained unchanged. These calculations indicate that flow-extended VWF bound, respectively, ADAMTS13 and MP-TSP6 with 6.7- and 14-fold higher affinities than coiled VWF.

To analyze the waiting time and bond lifetime data measured from the BFP thermal fluctuation assay, pooled waiting times t_w and bond lifetimes t_b were respectively fitted by the following equations for single-step irreversible association and dissociation of single monomeric bonds (Chen *et al.*, 2008a,b):

$$P_a = 1 - \exp\left(-m_r m_l A_c k_{on} t_w\right) \quad (2)$$

$$P_b = \exp\left(-k_{off}^0 t_b\right) \quad (3)$$

Combined with the molecular densities on beads, the effective on-rate A_ck_{on} can be derived from the fitting.

Measurement of molecular densities on beads

Beads coated with A1A2A3 or ADAMTS13 variants were respectively incubated with mouse anti-A1 mAb 5D2 or goat anti-ADAMTS13 polyclonal antibody 151 (for ADAMTS13 and MP-TSP6) or 158 (for CUB) at room temperature for 30 min, washed three times with HEPES containing 1% BSA, incubated with respective PE-conjugated goat-anti-mouse or rabbit-anti-goat antibody at room temperature for 30 min, washed three times with HEPES containing 1% BSA, and analyzed by a BD LSR flow cytometer (BD Biosciences). The number of molecules per bead was determined from the fluorescence intensity after calibration by standard beads (BD Quantibrite PE Beads). The site density was obtained by dividing the total number of molecules by the surface area of the bead.

Statistical tests

We used 50 touches to measure one adhesion frequency value from each spot. The numbers of spots (*n* values) are reported in the figure legends. The variability of spot-to-spot is indicated using box and whisker plots.

For statistics, a standard two-tailed Student's *t* test was performed to test the difference in adhesion frequency and VWF length between paired conditions. The *p* values below 0.05 were deemed statistically significant and are denoted by *. **, ***, and **** for $p < 0.05$, 0.01, 0.001, and 0.0001, respectively.

ACKNOWLEDGMENTS

We thank Tao Wu for his contributions in the early phase of this project and Michael Berndt for the generous gift of the 5D2 antibody. This work was supported by National Institutes of Health Grants HL132019 (C.Z.) and HL085769 and HL125957 (J.-f.D.), National Natural Science Foundation of China Grants 11432006 (J.W.) and 31500759 (J.L.), and Guangzhou Science Technology Program 201707010062 (J.L.).

REFERENCES

Akiyama M, Takeda S, Kokame K, Takagi J, Miyata T (2009). Crystal structures of the noncatalytic domains of ADAMTS13 reveal multiple discontinuous exosites for von Willebrand factor. Proc Natl Acad Sci USA 106, 19274–19279.

Auton M, Sowa KE, Smith SM, Sedlak E, Vijayan KV, Cruz MA (2010). Destabilization of the A1 domain in von Willebrand factor dissociates the A1A2A3 tri-domain and provokes spontaneous binding to glycoprotein Ibalpha and platelet activation under shear stress. J Biol Chem 285, 22831–22839.

Banno F, Chauhan AK, Kokame K, Yang J, Miyata S, Wagner DD, Miyata T (2009). The distal carboxyl-terminal domains of ADAMTS13 are required for regulation of in vivo thrombus formation. Blood 113, 5323–5329.

Banno F, Kaminaka K, Soejima K, Kokame K, Miyata T (2004). Identification of strain-specific variants of mouse Adamts13 gene encoding von Willebrand factor-cleaving protease. J Biol Chem 279, 30896–30903.

Chen W, Evans EA, McEver RP, Zhu C (2008a). Monitoring receptor-ligand interactions between surfaces by thermal fluctuations. Biophys J 94, 694–701.

Chen W, Lou J, Zhu C (2010). Forcing switch from short- to intermediate- and long-lived states of the αA domain generates LFA-1/ICAM-1 catch bonds. J Biol Chem 285, 35967–35978.

Chen W, Zarnitsyna VI, Sarangapani KK, Huang J, Zhu C (2008b). Measuring receptor–ligand binding kinetics on cell surfaces: from adhesion frequency to thermal fluctuation methods. Cell Mol Bioeng 1, 276–288.

Chesla SE, Selvaraj P, Zhu C (1998). Measuring two-dimensional receptor–ligand binding kinetics by micropipette. Biophys J 75, 1553–1572.

Crawley JTB, de Groot R, Xiang Y, Luken BM, Lane DA (2011). Unraveling the scissile bond: how ADAMTS13 recognizes and cleaves von Willebrand factor. Blood 118, 3212–3221.

de Groot R, Bardhan A, Ramroop N, Lane DA, Crawley JT (2009). Essential role of the disintegrin-like domain in ADAMTS13 function. Blood 113, 5609–5616.

De Marco L, Girolami A, Zimmerman TS, Ruggeri ZM (1986). Von Willebrand factor interaction with the glycoprotein IIb/IIa complex. Its role in platelet function as demonstrated in patients with congenital afibrinogenemia. J Clin Invest 77, 1272–1277.

Dong, JF (2005). Cleavage of ultra-large von Willebrand factor by ADAMTS-13 under flow conditions. J Thromb Haemost 3, 1710–1716.

Feys HB, Anderson PJ, Vanhoorelbeke K, Majerus EM, Sadler JE (2009). Multi-step binding of ADAMTS-13 to von Willebrand factor. J Thromb Haemost 7, 2088–2095.

Franchini M, Lippi G (2006). Von Willebrand factor and thrombosis. Ann Hematol 85, 415–423.

Furlan M, Robles R, Lammle B (1996). Partial purification and characterization of a protease from human plasma cleaving von Willebrand factor to fragments produced by in vivo proteolysis. Blood 87, 4223–4234.

Gao W, Anderson PJ, Majerus EM, Tuley EA, Sadler JE (2006). Exosite interactions contribute to tension-induced cleavage of von Willebrand factor by the antithrombotic ADAMTS13 metalloprotease. Proc Natl Acad Sci USA 103, 19099–19104.

Gao W, Anderson PJ, Sadler JE (2008). Extensive contacts between ADAMTS13 exosites and von Willebrand factor domain A2 contribute to substrate specificity. Blood 112, 1713–1719.

Gardner MD, Chion CK, de Groot R, Shah A, Crawley JT, Lane DA (2009). A functional calcium-binding site in the metalloprotease domain of ADAMTS13. Blood 113, 1149–1157.

Gustafsson MG (2005). Nonlinear structured-illumination microscopy: wide-field fluorescence imaging with theoretically unlimited resolution. Proc Natl Acad Sci USA 102, 13081–13086.

Ju L, Chen Y, Rushdi MN, Chen W, Zhu C (2017). Two-dimensional analysis of cross-junctional molecular interaction by force probes. Methods Mol Biol 1584, 231–258.

Ju L, Dong JF, Cruz MA, Zhu C (2013). The N-terminal flanking region of the A1 domain regulates the force-dependent binding of von Willebrand factor to platelet glycoprotein Ibα. J Biol Chem 288, 32289–32301.

Marshall BT, Long M, Piper JW, Yago T, McEver RP, Zhu C (2003). Direct observation of catch bonds involving cell-adhesion molecules. Nature 423, 190–193.

Muia J, Zhu J, Greco SC, Vanhoorelbeke K, Gupta G, Westfield LA, Sadler JE (2019). Phylogenetic and functional analysis of ADAMTS13 identifies highly conserved domains essential for allosteric regulation. Blood 133, 1899–1908.

Muia J, Zhu J, Gupta G, Haberichter SL, Friedman KD, Feys HB, Deforche L, Vanhoorelbeke K, Westfield LA, Roth R (2014). Allosteric activation of ADAMTS13 by von Willebrand factor. Proc Natl Acad Sci USA 111, 18584–18589.

Ruggeri ZM, Mendolicchio GL (2015). Interaction of von Willebrand factor with platelets and the vessel wall. Hamostaseologie 35, 211–224.

Schneider S, Nuschele S, Wixforth A, Gorzelanny C, Alexander-Katz A, Netz R, Schneider M (2007). Shear-induced unfolding triggers adhesion of von Willebrand factor fibers. Proc Natl Acad Sci USA 104, 7899–7903.
Schneppenheim R, Hellermann N, Brehm MA, Klemm U, Obser T, Huck V, Schneider SW, Denis CV, Tischer A, Auton M (2019). The von Willebrand factor Tyr2561 allele is a gain-of-function variant and a risk factor for early myocardial infarction. Blood 133, 356–365.
South K, Freitas MO, Lane DA (2017). A model for the conformational activation of the structurally quiescent metalloprotease ADAMTS13 by von Willebrand factor. J Biol Chem 292, 5760–5769.
South K, Luken BM, Crawley JT, Phillips R, Thomas M, Collins RF, Deforche L, Vanhoorelbeke K, Lane DA (2014). Conformational activation of ADAMTS13. Proc Natl Acad Sci USA 111, 18578–18583.
Tao Z, Peng Y, Nolasco L, Cal S, Lopez-Otin C, Li R, Moake JL, Lopez JA, Dong JF (2005). Recombinant CUB-1 domain polypeptide inhibits the cleavage of ULVWF strings by ADAMTS13 under flow conditions. Blood 106, 4139–4145.
Tsai H (1996). Physiologic cleavage of von Willebrand factor by a plasma protease is dependent on its conformation and requires calcium ion. Blood 87, 4235–4244.
Tsai HM (2007). Thrombotic thrombocytopenic purpura: a thrombotic disorder caused by ADAMTS13 deficiency. Hematol Oncol Clin North Am 21, 609–632, v.
Wayman AM, Chen W, McEver RP, Zhu C (2010). Triphasic force dependence of E-selectin/ligand dissociation governs cell rolling under flow. Biophys J 99, 1166–1174.
Wu T, Lin J, Cruz MA, Dong JF, Zhu C (2010). Force-induced cleavage of single VWFA1A2A3 tridomains by ADAMTS-13. Blood 115, 370–378.
Xu AJ, Springer TA (2012). Calcium stabilizes the von Willebrand factor A2 domain by promoting refolding. Proc Natl Acad Sci USA 109, 3742–3747.
Yago T, Wu JH, Wey CD, Klopocki AG, Zhu C, McEver RP (2004). Catch bonds govern adhesion through L-selectin at threshold shear. J Cell Biol 166, 913–923.
Zanardelli S, Chion AC, Groot E, Lenting PJ, McKinnon TA, Laffan MA, Tseng M, Lane DA (2009). A novel binding site for ADAMTS13 constitutively exposed on the surface of globular VWF. Blood 114, 2819–2828.
Zhang P, Pan W, Rux AH, Sachais BS, Zheng XL (2007). The cooperative activity between the carboxyl-terminal TSP1 repeats and the CUB domains of ADAMTS13 is crucial for recognition of von Willebrand factor under flow. Blood 110, 1887–1894.
Zhang X, Halvorsen K, Zhang CZ, Wong WP, Springer TA (2009). Mechanoenzymatic cleavage of the ultralarge vascular protein von Willebrand factor. Science 324, 1330–1334.
Zheng X, Chung D, Takayama TK, Majerus EM, Sadler JE, Fujikawa K (2001). Structure of von Willebrand factor-cleaving protease (ADAMTS13), a metalloprotease involved in thrombotic thrombocytopenic purpura. J Biol Chem 276, 41059–41063.
Zheng X, Nishio K, Majerus EM, Sadler JE (2003). Cleavage of von Willebrand factor requires the spacer domain of the metalloprotease ADAMTS13. J Biol Chem 278, 30136–30141.
Zhu J, Muia J, Gupta G, Westfield LA, Vanhoorelbeke K, Tolia NH, Sadler JE (2019). Exploring the "minimal" structure of a functional ADAMTS13 by mutagenesis and small-angle X-ray scattering. Blood 133, 1909–1918.